

MASS-DEPENDENT COLOR EVOLUTION OF FIELD GALAXIES BACK TO  $Z \sim 3$  OVER THE WIDE RANGE OF STELLAR MASS

M. KAJISAWA AND T. YAMADA

National Astronomical Observatory of Japan,  
2-21-1, Osawa, Mitaka, Tokyo 181-8588, Japan*Draft version December 2, 2024*

## ABSTRACT

We use deep multi-band optical and near-infrared data for four general fields, GOODS-South, HDF North/South, and IRAC UDF in GOODS-North to investigate the evolution of the observed rest-frame  $U - V$  color of field galaxies as a function of the stellar mass evaluated by fitting the galaxy spectral models to the observed broad-band SEDs. In these four fields, the  $U - V$  color distributions of the galaxies at each mass and redshift interval are very similar. At  $0.3 < z < 2.7$ , we found that more massive galaxies always tend to have a redder  $U - V$  color. High- and low-mass galaxies exhibit quite different color evolutions. As seen in our previous study in HDF-N, the color distribution of low-mass ( $M_{\text{stellar}} \lesssim 3 \times 10^9 M_{\odot}$ ) galaxies becomes significantly bluer with an increase in the redshift. This evolution of the average color can be explained by a constant star formation rate model with  $z_{\text{form}} \sim 4$ . On the other hand, the average color of high-mass galaxies ( $M_{\text{stellar}} \gtrsim 3 \times 10^{10} M_{\odot}$ ) evolves more strongly at a high redshift. Such mass-dependent color distribution and its evolution indicate that galaxies with a larger stellar mass appear to have shorter star-formation timescales, and on an average, they form the larger fraction of their stars in the earlier epoch.

*Subject headings:* galaxies: evolution — galaxies: formation — galaxies: high-redshift

## 1. INTRODUCTION

Stellar mass is one of the most important quantities of galaxies that facilitate the understanding of their formation and evolution. The evolution of the number density of galaxies as a function of the stellar mass conveys the overall history of star formation and the mass assembly process in the universe. Many authors have investigated such evolution of the stellar mass distribution function back to  $z \gtrsim 1$  (e.g., Dickinson, Papovich, Ferguson, & Budavári 2003, Bell et al. 2003, Fontana et al. 2004, Drory et al. 2004, Drory et al. 2005).

On the other hand, the study of properties such as the spectral energy distribution (SED), colors, and line fluxes of galaxies as a function of the stellar mass at various epochs helps us to understand star formation histories in additional detailed, such as, in what manner the star formation occurs in low- and high-mass galaxies and how it contributes to the growth of their stellar mass. In the case of local galaxies detected in the Sloan Digital Sky Survey, Heavens et al. (2004) and Jimenez et al. (2005) argued that most of the stars in the present-day massive galaxies have been formed at a high redshift, while star formation histories of low-mass galaxies have relatively longer timescales. In more direct observations of high-redshift galaxies, Cowie et al. (1996) originally found that the mass of the galaxies undergoing rapid star formation has been declining smoothly with a decrease in the redshift. Recently, Juneau et al. (2005) also investigated the stellar mass dependence of star formation rates of galaxies at  $0.8 < z < 2.0$  using the Gemini Deep Deep Survey data. They found the trend to be similar to that predicted in the studies of local galaxies (Heavens et al. 2004). Similar results are obtained in the studies on the evolution of specific star formation rates back to  $z \sim 1$

1.5 (Brinchmann & Ellis 2000, Bauer et al. 2005, Feulner et al. 2005a). Very recently, Feulner et al. (2005b) extended the analysis to  $z \sim 5$ , and found that a similar trend continues even at a higher redshift.

The samples in these previous studies, however, are too shallow to reach a sufficiently low mass range below  $\sim 5 \times 10^9 M_{\odot}$ , a characteristic “transition” mass (Kajisawa and Yamada 2005, and Section 4 below), or are biased toward objects with typically low M/L ratios, such as more actively star-forming bluer populations due to the lack of very deep near-infrared (NIR) data. The evolution of low-mass galaxies is, however, important to understand the overall picture of galaxy evolution not only because they may be the building blocks of more massive galaxies but also because they are more sensitive probes to understand the thermal history of the universe.

In Kajisawa and Yamada (2005, hereafter referred to as KY05), we investigated the evolution of the rest-frame color and morphology distribution of the galaxies in HDF-N as a function of the stellar mass back to  $z \sim 3$  over a wide range of stellar masses down to  $10^9 M_{\odot}$ . We found that the behavior of the rest-frame  $U - V$  color distribution and its dependence on the stellar mass change at around  $\sim 5 \times 10^9 M_{\odot}$ . In addition, we discovered that the sequence of the color distribution of low-mass galaxies systematically becomes bluer with the redshift, while the colors of high-mass galaxies do not show a significant redshift evolution. However, the area of the HDF-N data used in our analysis was only  $\sim 3.5 \text{ arcmin}^2$ , and it was inferred that the effect of field-to-field variation was large.

Therefore, in this paper, we have extended the study area of KY05 to include some other fields, GOODS-S (Giavalisco et al. 2004), a part of the IRAC Ultra Deep Field in GOODS-N (Dickinson et al. 2003b), and FIRE (HDF-South, Labb   et al. 2003). Using the deep optical

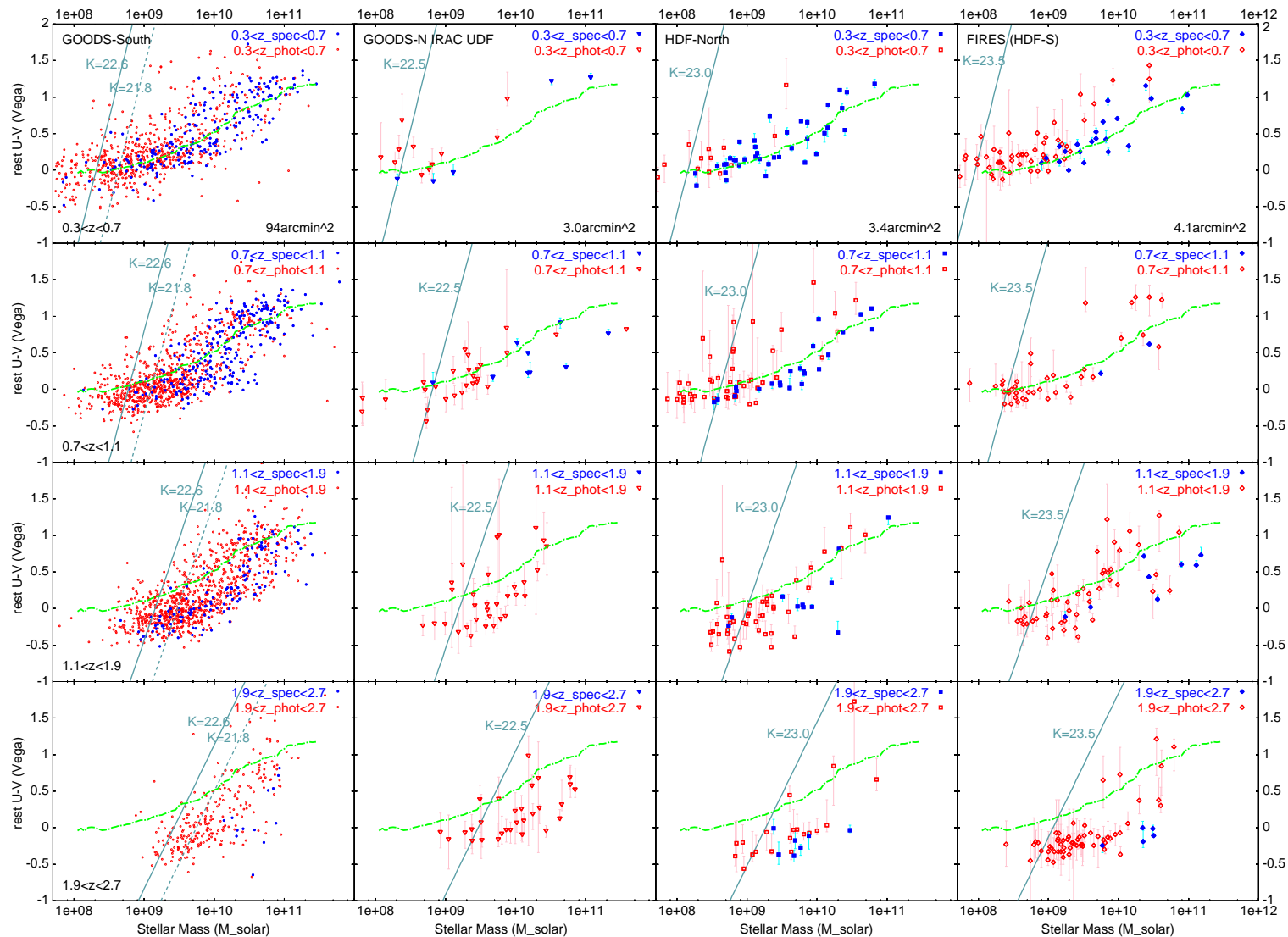


FIG. 1.— Rest-frame  $U - V$  color distribution as a function of stellar mass of  $K$ -selected galaxies. Each row depicts different redshift bin, and each column depicts different fields. Blue symbols indicate objects with spectroscopic redshift, while red ones indicate the phot-z sample. Error bars show the range of 90% confidence level (the redshift uncertainty is considered for the phot-z sample). Solid lines (and dashed lines for the most shallow ISAAC field in GOODS-S) show the detection limit that corresponds to the 90% completeness limit for point sources (see KY05 for the method of estimating the lines). The dotted-dash lines show the weighted average for the GOODS-S sample at  $0.3 < z < 0.7$  (top-left panel).

and NIR data for these fields, we investigate the rest-frame  $U - V$  color evolution of galaxies at  $0.3 < z < 2.7$  as a function of the stellar mass. These data allow us to extend our previous analysis to a larger sample in order to study the evolution of galaxies with a high statistical accuracy. We used the Vega magnitude system throughout the paper.

## 2. DATA & SOURCE DETECTION

We used multi-band optical and NIR data in the four fields, GOODS-S, FIRE, HDF-N, and a part of IRAC UDF in GOODS-N. For HDF-N, we used the same data as those used in KY05 (HST/WFPC2, HST/NICMOS, Subaru/CISCO, UBVJHK set). For GOODS-S, we used the publicly available VLT/ISAAC ver1.5 data (JHK-bands) and HST/ACS ver1.0 data (bviz, Giavalisco et al. 2004). For FIRE, we used the publicly available HST/WFPC2 + VLT/ISAAC data (UBVJHK, Labbe et al. 2003).

For IRAC UDF in GOODS-N, we observed a field in the  $J$  and  $K$  bands using the Subaru Telescope equipped with CISCO (Motohara et al. 2002) on March 10, 2003. The field of view (FOV) used in the analysis was  $1.74' \times 1.74'$ , and the total exposure time in the  $K$  and  $J$  bands was 14780 and 3880 s, respectively. The data were reduced using the IRAF software package, as described in KY05. The publicly available GOODS HST/ACS ver1.0 data (bviz) were also used in the field.

For all the fields, we independently performed source detection in the  $K$ -band images using the SExtractor image analysis package (Bertin & Arnouts 1996). We adopted MAG\_AUTO from SExtractor as the total magnitude of the detected objects. The SED (colors) was measured in the optimal-S/N aperture size for each galaxy (see KY05 for details). We excluded regions with lower sensitivity, such as the edge region of each ISAAC FOV for GOODS-S, from our analysis. The areas in the analyses were 94 arcmin<sup>2</sup> for GOODS-S, 3.0 arcmin<sup>2</sup> for IRAC UDF, 3.4 arcmin<sup>2</sup> for HDF-N, and 4.1 arcmin<sup>2</sup> for FIRE. We performed simulations using the IRAF/ARTDATA package to quantify the depth of each field. The 90% completeness limit for the point source is  $K \sim 21.8\text{--}22.6$  ( $\sim 21.4$  for one FOV) for GOODS-S,  $K \sim 22.5$  for IRAC UDF,  $K \sim 23.0$  for HDF-N, and  $K \sim 23.5$  for FIRE.

## 3. ANALYSIS

Using these optical and NIR photometric data, we measured the redshift, the stellar mass, and the rest-frame  $U - V$  color of each galaxy in the same manner as that in KY05. When possible, we used the spectroscopic redshifts from literature (Szokoly et al. 2004, Le Fèvre et al. 2004, Vanzella et al. 2005, Wirth et al. 2004, Cohen et al. 2000, Labbè et al. 2003). For objects without spectroscopic identification, we estimated the photometric redshifts using the publicly available “hyperz” code (Bolzonella et al. 2000) in the same manner as that in KY05; however, for FIRE, we used the publicly available phot-z catalogue (Labbè et al. 2003).

After the redshifts were determined, we performed a detailed SED fitting with the GALAXEV synthetic library (Bruzual & Charlot 2003) in order to measure the stellar mass and the rest-frame color of the galaxies. We assumed IMF of Chabrier (2003), exponentially decaying

SFR, and the extinction law of Calzetti et al. (2000). The free parameters were the age, star formation timescale, color excess, and metallicity. The fitting results were used to estimate the M/L ratio (and subsequently, the stellar mass) and measure the K-correction values for the rest-frame colors. The parameter range of dust extinction is  $0 \leq E(B - V) \leq 0.62$ , and the median of the best-fitted values is 0.13 (about 75% of the samples had  $E(B - V) < 0.3$ ). Additional details of the procedures and the discussion on the uncertainty of the mass and color evaluation are described in KY05. It should be noted that although each parameter such as dust extinction, stellar age, or star formation timescale is not constrained very tightly, the stellar mass can be estimated with a relatively low uncertainty. This is because the effects of these parameters tend to cancel out in the estimation of the stellar mass, as discussed in KY05 (see also Papovich, Dickinson, & Ferguson 2001 for a detailed discussion). In addition, note that the rest-frame  $U - V$  color is measured from the observed photometric data without extrapolation. Therefore, the stellar mass and the  $U - V$  color used in the current analysis are robust quantities.

## 4. RESULTS & DISCUSSION

In Figure 1, for each of the four fields, we plotted the rest-frame  $U - V$  color of the K-selected galaxies in each redshift bin as a function of the stellar mass. First, we can see from this figure that the color distributions of the galaxies in the four fields are very similar. For reference, we estimated the weighted mean colors with a bin of  $\pm 0.15$  dex of the GOODS-S sample at  $0.3 < z < 0.7$  (in the top-left panel), and plotted them in all the panels by dotted-dash lines. The  $U - V$  color is always very blue for  $M_{\text{stellar}} \lesssim 10^9 M_{\odot}$  and becomes redder as the stellar mass increases toward  $\sim 10^{11} M_{\odot}$ . Most of the galaxies with  $M_{\text{stellar}} \gtrsim 10^{11} M_{\odot}$  have the reddest color.

In fact, it is evident from Figure 1 that over the entire redshift range at  $0.3 < z < 2.7$ , the more massive galaxies always have the redder  $U - V$  color. For example, while most of the galaxies with  $M_{\text{stellar}} \lesssim 3 \times 10^9 M_{\odot}$  have  $U - V < 0.3$  at any redshift, many objects with  $M_{\text{stellar}} \gtrsim 3 \times 10^{10} M_{\odot}$  have  $U - V \sim 1$ . This trend is consistent with the results found in Feulner et al. (2005b) and other previous studies. If we observe the redshift evolution in Figure 1 more closely, we notice the gradual bluing of the  $U - V$  color along the redshift within the mass range of  $10^9 M_{\odot} \lesssim M_{\text{stellar}} \lesssim 10^{10} M_{\odot}$ . While this systematic evolution of the rest-frame color distribution of low-mass galaxies has already been reported in KY05 for HDF-N, it is now confirmed by the larger sample that includes three other different fields.

In Figure 2, we try to quantify the observed mass-dependent color evolution by using an analytical fitting function. The data for all the four fields are combined. We excluded the lowest mass galaxies in each field from the sample so that the color bias near the detection limit (solid lines in Figure 1) does not affect the fitting significantly; the limiting masses are set so that the  $K$ -band source detection completeness at  $U - V \sim 0.8$  is 50%. These limiting stellar masses are tabulated in Table 1. Considering the shape of the mass-weighted average color profile in GOODS-S (the top-left panel in Figure 1), we chose a hyperbolic tangent as the fitting function.

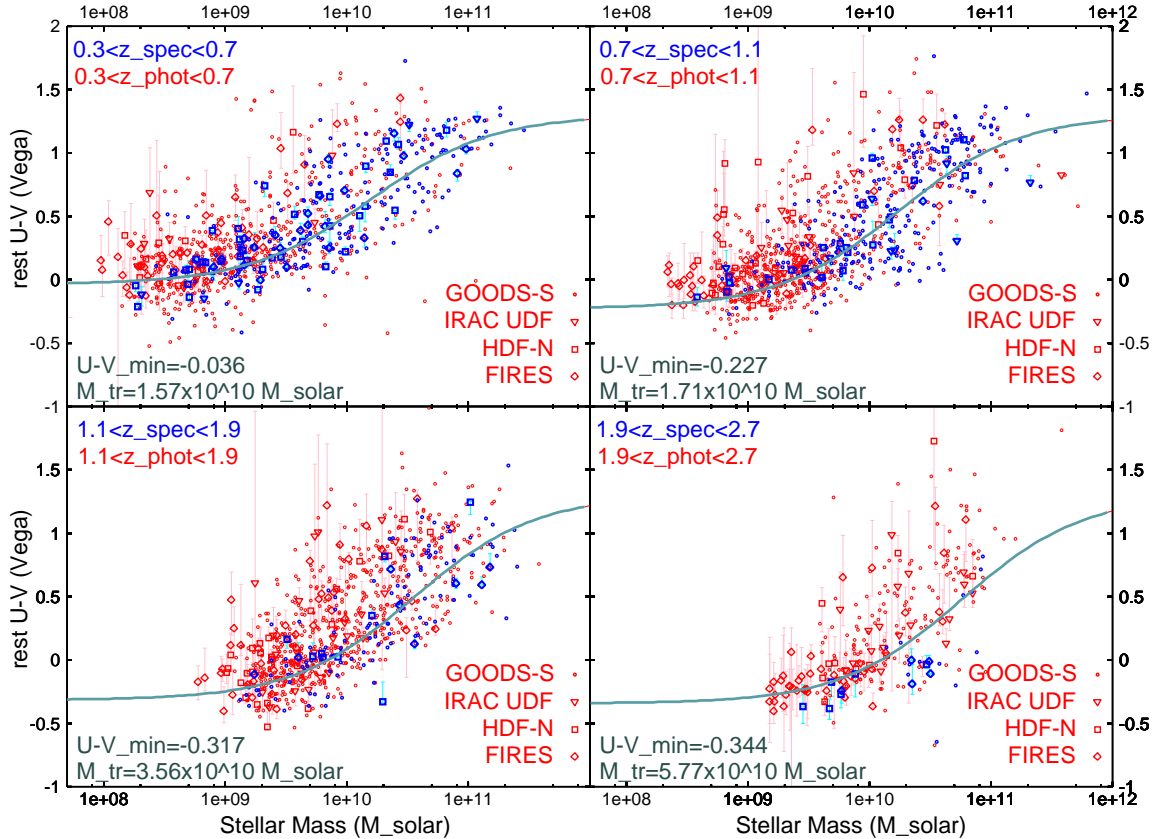


FIG. 2.— Rest-frame  $U - V$  color distribution as a function of the stellar mass for the sum of all the four fields in each redshift bin. Data from different fields are plotted by different symbols. Blue and red symbols represent the spec-z and phot-z samples, respectively. Solid lines show the fitted “tanh” function in each redshift bin. The fitting parameters,  $UV_{MIN}$  and  $M_{tr}$  (see text) are also shown.

TABLE 1  
LOWER LIMIT OF STELLAR MASS IN EACH FIELD ( $M_{\odot}$ )

Redshift	GOODS-South	IRAC UDF	HDF-N	FIRES
0.3-0.7	$1.4-3.3 \times 10^8$	$1.8 \times 10^8$	$1.1 \times 10^8$	$6.6 \times 10^7$
0.7-1.1	$4.2-10 \times 10^8$	$5.5 \times 10^8$	$3.5 \times 10^8$	$2.0 \times 10^8$
1.1-1.9	$1.2-2.9 \times 10^9$	$1.6 \times 10^9$	$1.0 \times 10^9$	$5.8 \times 10^8$
1.9-2.7	$3.1-7.6 \times 10^9$	$4.1 \times 10^9$	$2.6 \times 10^9$	$1.5 \times 10^9$

This was in keeping with Baldry et al. (2004) who used a similar form to quantify the bimodality in the color-magnitude distribution of the SDSS sample. The fitting function is written as follows:

$$U - V(M_{stellar}) = \left( \frac{UV_{MIN} + UV_{MAX}}{2} \right) + \left( \frac{UV_{MAX} - UV_{MIN}}{2} \right) \times \tanh(R(M_{stellar} - M_{tr}))$$

where  $UV_{MIN}$  and  $UV_{MAX}$  are the asymptotic minimum and maximum values of the rest-frame  $U - V$  color at the low- and high-mass ends.  $M_{tr}$  and  $R$  represent the mass and mass range at which the color transition occurs. For simplicity, we fixed  $R$  and  $UV_{MAX}$ , which seem to change little with the redshift in our sample, to the values fitted at  $0.3 < z < 0.7$  ( $R = 1.0$ ,  $UV_{MAX} = 1.3$ ). Next, we fitted the color distribution in each redshift bin by changing the values of  $M_{tr}$  and  $UV_{MIN}$ . The result is shown by the solid lines in Figure 2. The best-fitted values of the parameters are  $M_{tr} = 1.57^{+0.39}_{-0.23} \times 10^9 M_{\odot}$  and  $UV_{MIN} = -0.036 \pm 0.055$  at  $0.3 < z < 0.7$ ,  $M_{tr} = 1.71^{+0.28}_{-0.24} \times 10^9 M_{\odot}$

and  $UV_{MIN} = -0.277 \pm 0.056$  at  $0.7 < z < 1.1$ ,  $M_{tr} = 3.56^{+1.09}_{-0.84} \times 10^9 M_{\odot}$  and  $UV_{MIN} = -0.317 \pm 0.128$  at  $1.1 < z < 1.9$ ,  $M_{tr} = 5.77^{+1.79}_{-1.37} \times 10^9 M_{\odot}$  and  $UV_{MIN} = -0.344 \pm 0.084$  at  $1.9 < z < 2.7$ . These results again show that the  $U - V$  color at the low-mass end gradually evolves blueward with the redshift. In addition, the transition mass also seems to increase along the redshift, although the uncertainty is relatively large. It is noteworthy that Bundy et al. (2006) also recently discovered similar transition mass increments with the redshift at  $0.4 < z < 1.4$  in the study using the DEEP2 data.

Figure 3 shows the evolution of the rest-frame  $U - V$  color at each stellar mass range for the combined data. We plotted the weighted average colors binned over the redshift range of  $\pm 0.15$  (dotted-dash lines). In the top panel, it is more clearly evident that the color distribution of the galaxies with  $M_{stellar} < 3 \times 10^9 M_{\odot}$  becomes gradually bluer with an increase in the redshift. In KY05, we discussed that the star formation activity in these low-mass galaxies occurs rather continuously since they exhibit a very blue color at *any* redshift. A bluer color even at a higher redshift also suggests younger average ages of the galaxies at  $z = 2-3$ . In the lower panels, we see that the colors of galaxies with a larger stellar mass also become bluer at a high redshift. There seems to be a trend where the more massive populations show

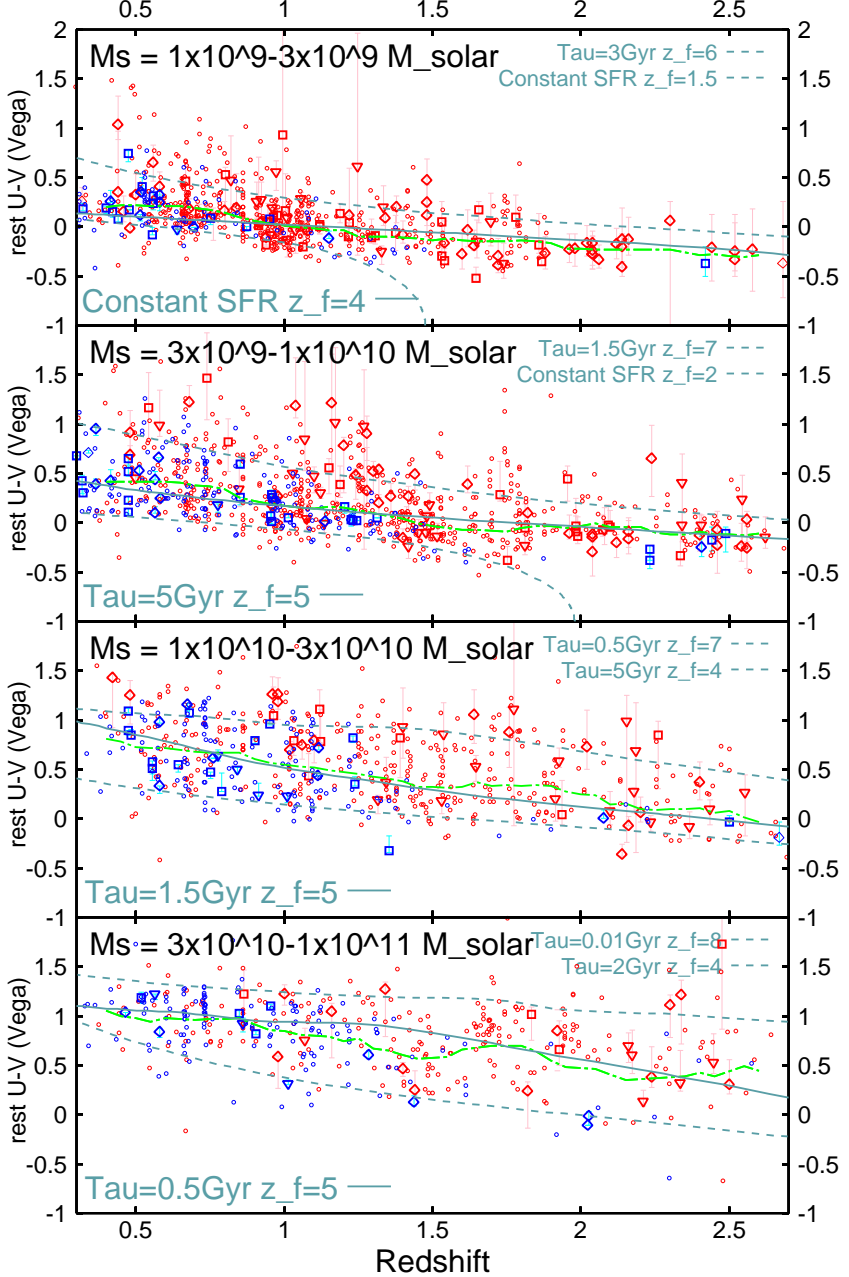


FIG. 3.— rest-frame  $U - V$  color vs redshift for galaxies within each stellar mass range. The plotted sample and the meaning of the symbols are similar to those in Figure 2. Dotted-dash lines and solid lines show the weighted average and the best-fit GALAXEV models with exponentially decaying SFR. Dashed lines show the upper and lower envelope of the color distribution.

a stronger color evolution at a high redshift, which in fact corresponds to the evolution of the transition mass found in Figure 2.

We try to fit such color evolutions using GALAXEV population synthesis models with simple star formation histories. We simply consider an exponentially decaying SFR and assume solar metallicity and no dust extinction. We estimate the  $U - V$  color for the model grid with the star formation timescale  $\tau = 0.01, 0.05, 0.1, 0.5, 1, 1.5, 2, 3, 5, 15$ , and  $\infty$  (constant SFR) Gyr and the formation redshift  $z_f = 3, 4, 5, 6, 7$ , and 8. Eventually, we found that  $\tau$  mainly affects the overall slope of the color evolu-

tion, and  $z_f$  strongly affects the color at a high redshift (e.g.,  $z > 2$ ). The resultant best-fit models and their  $\tau$  and  $z_f$  values are shown in Figure 3. It is found from the results that the more massive populations appear to have a shorter star formation timescale. In other words, they form the larger fraction of their stellar contents at a high redshift. Such a trend is very similar to the concept of mass-dependent star formation histories argued by Heavens et al. (2004). Further, the trend is also consistent with the studies on mass-dependent evolutions of specific star formation rates at a high redshift (Feulner et al. 2005b, Juneau et al. 2005). However, in this study,

the trend is depicted by more directly observable quantities.

In these analyses, it is important to check the effect of the color bias near the detection limit. The bias against a red high-M/L population is expected to be severe, especially for low-mass galaxies at a high redshift since the  $K$ -band filter samples relatively short rest-frame wavelengths. We finally discovered, however, that our deep  $K$ -selected samples do not suffer considerably from the bias. It is true that our 50% completeness limit at  $U - V = 0.8$  could neglect some fractions of relatively red low-mass galaxies in the highest redshift bin. However, the color distribution tends to concentrate at considerably bluer values ( $U - V \lesssim 0$ ), and there is few galaxies that are redder than  $U - V = 0.3$ , where the completeness is greater than 90%. This can be demonstrated by the lowest mass objects near the detection limit ( $K \sim 23.5$ ) in the highest redshift bin of the deepest FIREs data. For example, out of 20 galaxies with the stellar mass of  $1.5 \times 10^9 M_{\odot} < M_{\text{stellar}} < 3.0 \times 10^9 M_{\odot}$  in the  $1.9 < z < 2.7$  bin of FIREs, 19 galaxies have  $U - V < 0$ , and one galaxy has  $0 < U - V < 0.1$ ; further, no galaxy has  $0.1 < U - V < 0.3$ .

Indeed, a sample selection with very deep NIR data is essential not only for evaluating the stellar mass of galaxies but also for generating relatively unbiased samples to study the color distribution of these low-mass galaxies at a high redshift. For example,  $I$ -band selections such as those used for the FORS Deep Field data in Feulner et al. (2005b) could introduce a severe color bias. The detection limit of  $I(AB) = 26.4$  in Feulner et al. (2005b) can only sample galaxies with  $U - V < -0.1$  for  $M_{\text{stellar}} = 2 \times 10^9 M_{\odot}$  at  $z > 2$ . Such a selection does not reveal whether red galaxies exist.

In Figure 3, we found that the stronger color evolution of massive galaxies at a high redshift was explained by the exponentially decaying SFR models with  $z_f \sim 4-5$ , for which the star formation timescale decreases with mass. On the other hand, the evolution of the average color of low-mass ( $\lesssim 3 \times 10^9 M_{\odot}$ ) galaxies can actually be explained by the constant SFR model. However, the best-fit formation redshift occurs at  $z_f \sim 4$ , which is similar to those for high-mass galaxies. If this is true, the differences in the star formation histories among galaxies with different stellar masses are not mainly in the epochs when the star formation began, but rather, in the

star formation efficiencies and/or mechanisms by which star formation activities are suppressed. The long star-formation timescale for low-mass galaxies can be caused by the self-regulation of star formation, for example, by a supernova feedback (Dekel & Birnboim 2005). The mass dependence of the star formation efficiencies and suppression mechanisms can be related with processes such as the efficient exhaustion of gas reservoirs (e.g., Menci et al. 2005) or shock heating of cold gas during a major merger (Cox et al. 2004).

It is noteworthy that some of the assumptions in our analysis may be oversimplifications. If we consider dust extinction, the estimated formation redshift shifts to smaller values. For example, if we assume the extinction of  $E(B - V) = 0.13$  (median-fitted value of our sample) for low-mass galaxies, the best-fit formation redshift of these galaxies shifts from  $z_f = 4$  to  $z_f = 3$ . We also verified which variations of star formation histories are permissible if the scatter of the colors around the average values is considered. To illustrate this, we plotted the GALAXEV models that trace the upper and lower envelopes of the color distribution by dashed lines in each panel in Figure 3.

Finally, we note that several other surveys have investigated the evolution of the stellar mass or luminosity function of field galaxies and found that the normalization decreases at  $z \gtrsim 1$  (e.g., Fontana et al. 2004, Yamada et al. 2005, Caputi et al. 2006, Saracco et al. 2006). Several studies have also suggested mass-dependent number density evolution (e.g., Glazebrook et al. 2004, Drory et al. 2004, Drory et al. 2005). The next step is to consistently explain both the color (SED) evolution and the number density evolution as functions of the stellar mass.

We wish to thank the anonymous referee for invaluable comments. This study is based on data collected at Subaru Telescope, which is operated by the National Astronomical Observatory of Japan. This study is also based on data collected at Very Large Telescope at the ESO Paranal Observatory under Program ID: LP168.A-0485. Data reduction/analysis was carried out on “sb” computer system operated by the Astronomical Data Analysis Center (ADAC) and Subaru Telescope of the National Astronomical Observatory of Japan.

## REFERENCES

- Baldry, I. K., Glazebrook, K., Brinkmann, J., Ivezić, Ž., Lupton, R. H., Nichol, R. C., & Szalay, A. S. 2004, ApJ, 600, 681  
 Bauer, A. E., Drory, N., Hill, G. J., & Feulner, G. 2005, ApJ, 621, L89  
 Bell, E. F., McIntosh, D. H., Katz, N., & Weinberg, M. D. 2003, ApJ, 585, L117  
 Bertin, E. & Arnouts, S. 1996, A&AS, 117, 393  
 Bolzonella, M., Miralles, J. M. & Pelló, R. 2000, A&A, 363, 476  
 Brinchmann, J. & Ellis, R. S. 2000, ApJ, 536, L77  
 Bruzual, G. & Charlot, S. 2003, MNRAS, 344, 1000  
 Bundy, K., et al., ApJ submitted, [astro-ph/0512465](http://arxiv.org/abs/astro-ph/0512465)  
 Calzetti, D., Armus, L., Bohlin, R. C., Kinney, A. L., Koornneef, J., & Storchi-Bergmann, T. 2000, ApJ, 533, 682  
 Caputi, K. I., McLure, R. J., Dunlop, J. P., Cirasuolo, M., & Schaefer, A. M. 2006, MNRAS, in press [astro-ph/0511571](http://arxiv.org/abs/astro-ph/0511571)  
 Chabrier, G. 2003, ApJ, 586, L133  
 Cohen, J. G., Hogg, D. W., Blandford, R., Cowie, L. L., Hu, E., Songaila, A., Shopbell, P., & Richberg, K. 2000, ApJ, 538, 29  
 Cowie, L. L., Songaila, A., Hu, E. M., & Cohen, J. G. 1996, AJ, 112, 839  
 Cox, T. J., Primack, J., Jonsson, P., & Somerville, R. S. 2004, ApJ, 607, L87  
 Dekel, A. & Birnboim, Y. 2005, ApJ, submitted [astro-ph/0412300](http://arxiv.org/abs/astro-ph/0412300)  
 Dickinson, M., Papovich, C., Ferguson, H. C., & Budavári, T. 2003, ApJ, 587, 25  
 Dickinson, M., Giavalisco, M., & The GOODS Team 2003b, The Mass of Galaxies at Low and High Redshift, 324  
 Drory, N., Bender, R., Feulner, G., Hopp, U., Maraston, C., Snigula, J., & Hill, G. J. 2004, ApJ, 608, 742  
 Drory, N., Salvato, M., Gabasch, A., Bender, R., Hopp, U., Feulner, G., & Pannella, M. 2005, ApJ, 619, L131  
 Feulner, G., Goranova, Y., Drory, N., Hopp, U., & Bender, R. 2005a, MNRAS, 358, L1  
 Feulner, G., Gabasch, A., Salvato, M., Drory, N., Hopp, U., & Bender, R. 2005b, ApJ, 633, L9  
 Fontana, A., et al. 2004, A&A, 424, 23  
 Giavalisco, M., et al. 2004, ApJ, 600, L93  
 Glazebrook, K., et al. 2004, Nature, 430, 181  
 Heavens, A., Panter, B., Jimenez, R., & Dunlop, J. 2004, Nature, 428, 625  
 Jimenez, R., Panter, B., Heavens, A. F., & Verde, L. 2005, MNRAS, 356, 495  
 Juneau, S., et al. 2005, ApJ, 619, L135  
 Kajisawa, M., & Yamada, T. 2005, ApJ, 618, 91 (KY05)

- Labbé, I., et al. 2003, AJ, 125, 1107  
Le Fèvre, O., et al. 2004, A&A, 428, 1043  
Menci, N., Fontana, A., Giallongo, E., & Salimbeni, S. 2005, ApJ, 632, 49  
Motohara, K., et al. 2002, PASJ, 54, 315  
Papovich, C., Dickinson, M., & Ferguson, H. C. 2001, ApJ, 559, 620  
Saracco, P., et al. 2006, MNRAS, in press *astro-ph/0512147*  
Szokoly, G. P., et al. 2004, ApJS, 155, 271  
Vanzella, E., et al. 2005, A&A, 434, 53  
Wirth, G. D., et al. 2004, AJ, 127, 3121  
Yamada, T., et al. 2005, ApJ, 634, 861